

# Craig’s XY–distribution and the statistics of Lagrangian power in two-dimensional turbulence

Mahesh Bandi<sup>1,\*</sup> and Colm Connaughton<sup>2,3,†</sup>

<sup>1</sup>*Condensed Matter and Thermal Physics Division & Center for Nonlinear Studies, LANL, Los Alamos, NM 87545, USA*

<sup>2</sup>*Theoretical Division & Center for Nonlinear Studies, LANL, Los Alamos, NM 87545, USA*

<sup>3</sup>*Centre for Complexity Science & Mathematics Institute,  
University of Warwick, Coventry CV4 7AL, UK*

(Dated: November 7, 2018)

We examine the probability distribution function (pdf) of energy injection rate (power) in numerical simulations of stationary two–dimensional (2D) turbulence in the Lagrangian frame. The simulation is designed to mimic an electromagnetically driven fluid layer, a well-documented system for generating two–dimensional turbulence in the laboratory. In our simulations, the forcing and velocity fields are close to Gaussian. On the other hand, the measured PDF of injected power is very sharply peaked at zero, suggestive of a singularity there, with tails which are exponential but asymmetric. Large positive fluctuations are more probable than large negative fluctuations. It is this asymmetry of the tails, which leads to a net positive mean value for the energy input despite the most probable value being zero. The main features of the power distribution are well described by Craig’s XY distribution for the PDF of the product of two correlated normal variables. We show that the power distribution should exhibit a logarithmic singularity at zero and decay exponentially for large absolute values of the power. We calculate the asymptotic behavior and express the asymmetry of the tails in terms of the correlation coefficient of the force and velocity. We compare the measured pdfs with the theoretical calculations and briefly discuss how the power pdf might change with other forcing mechanisms.

PACS numbers: 47.27.Gs

## INTRODUCTION

Since turbulence is an intrinsically dissipative phenomenon, it requires an external source of energy to sustain it. For a turbulent flow in a statistically stationary state, the rate of injection of energy into the system from this external energy source, the input power, is equal, *on average*, to the rate of dissipation of energy by small scale viscous processes. The fact that equality holds only on average is crucial. Since the input power is typically calculated as a product of an external force with the fluid velocity, both being fluctuating quantities, it is itself a fluctuating quantity with a full statistics of its own. Locally in space or in time this injected power need not balance the corresponding rate of dissipation. In fact it need not even remain positive.

Understanding the rate of energy injection in turbulence is of considerable importance in an engineering context, since it relates to the power required to overcome turbulent drag to sustain the rotation of a fan or turbine at a given speed in a turbulent flow (see, for example, [1]). In this context, much research focusses on the mean value of the power and how it scales with the Reynolds number. Such measurements, focussing on the mean power, in the context of Taylor–Couette flow were first performed by Lathrop et al. [2]. Subsequent research has focussed on measuring the pdf of the power fluctuations as well as the mean value in several turbulent systems including von-Kármán flows [3, 4], electro-convection [5], wave turbulence [6] and turbulent convection [7]. In this latter

case, it was the heat transfer rather than the power which was measured. Much of the recent work has focused on finding macroscopic non-equilibrium systems on which to test various non-equilibrium “Fluctuation Relations” [8, 9, 10] which have attracted much theoretical interest in recent years. In simple terms, these relations express a symmetry of the probability distribution of some time-integrated quantity associated with the dissipation or entropy production in a non-equilibrium system. For a review, see [11] and the references therein.

All of the works cited above have focused on measurements of the statistics of global quantities. All have observed non-trivial probability distributions, typically with exponential tails but, to date, most of the discussions of the power distribution have been qualitative. In this article we use the notion of Lagrangian turbulence as a local measure of the energy injection into a turbulent flow. We measure the probability distribution from numerical simulations and give a quantitative explanation of the observed distribution in terms of Craig’s XY-distribution for the product of correlated Gaussian variables. Although one can test the Fluctuation Relation for Lagrangian power fluctuations [12], this is not the purpose of the present article. We shall focus on the statistics of the power itself rather than its time integral.

The outline of the paper is as follows. We first give some background on turbulence in two dimensions, explaining the difference between the direct and inverse cascades. We then give some details of our numerical simulations and introduce the notion of Lagrangian mea-

measurements and the concept of Lagrangian power as a diagnostic of the energy injection into a turbulent flow. We then derive some asymptotic properties of the probability distribution of the product of two correlated normal variables (Craig’s XY-distribution). We then return to the turbulence data and explain our measurements of the Lagrangian power in terms of Craig’s XY-distribution.

## LAGRANGIAN TURBULENCE IN TWO DIMENSIONS

The physics of forced turbulence in 2D differs essentially from its three-dimensional counterpart. This difference can be traced to the presence of a second inviscid invariant in 2D, in addition to the energy. It is called enstrophy. The pivotal role of the enstrophy was first elucidated in seminal work by Kraichnan[13], Leith[14] and Batchelor [15] (KLB) which has since come to be considered as the classical theory of turbulence in 2D. The essential insight of the KLB theory is that simultaneous energy and enstrophy conservation requires the establishment of a second cascade with an independent dissipation mechanism if a stationary state is to be reached. In this dual-cascade picture, the enstrophy cascades from the forcing scale to smaller scales whereas the energy simultaneously cascades from the forcing scale to larger scales. This latter phenomenon, entirely absent in 3D, is known as an inverse cascade. Viscosity dissipates enstrophy at small scales whereas friction between the fluid layer and the substrate on which it moves (Ekman damping) dissipates energy at large scales. Assuming asymptotically large separation of the forcing and dissipation scales for both cascades, and applying standard Kolmogorov phenomenology[16], the KLB theory predicts that the energy spectrum in the direct cascade range should scale as  $k^{-3}$ , and in the inverse cascade range as  $k^{-5/3}$  where  $k$  is the modulus of the wave-vector,  $\vec{k}$ . These spectra carry constant fluxes of enstrophy or energy through their respective inertial ranges, that is, ranges of scales over which forcing and dissipation are negligible. This dual cascade theory has been shown to be in reasonable agreement with numerical simulations, provided that a sufficiently large inertial range is available to each cascade[17]. Experimentally, both the direct and inverse cascades have been observed[18]. While observing both cascades simultaneously is rather difficult, there is broad agreement that the KLB theory is correct asymptotically. See [19] for a review of experiments.

Much research has focused on the inverse cascade in isolation since it is responsible for the generation of large scale coherent motions in two dimensional flow and, despite the intertwining of the two cascades in the KLB theory, it is known to persist even when the direct cascade range is under-developed[20]. Numerical experiments[21] strongly support the  $k^{-5/3}$  scaling for the inverse cascade

spectrum, laboratory experiments [22] are consistent and the phenomenological KLB description of inverse energy transfer has been put in a firm quantitative basis[23].

We solve the incompressible Navier–Stokes equation with Ekman term for the 2D velocity field,  $\mathbf{v}(\mathbf{x}, t)$ :

$$\begin{aligned} \frac{\partial \mathbf{v}}{\partial t} + (\mathbf{v} \cdot \nabla) \mathbf{v} + \nabla p &= \nu \nabla^2 \mathbf{v} - \alpha \mathbf{v} + \mathbf{f} \\ \nabla \cdot \mathbf{v} &= 0. \end{aligned} \quad (1)$$

Here,  $\mathbf{f}(\mathbf{x}, t)$  is a forcing term (discussed below) and  $p(\mathbf{x}, t)$  is the pressure field. The parameters  $\nu$  (viscosity) and  $\alpha$  (Ekman friction coefficient) control the dissipation at small and large scales respectively. As a result of using physical dissipation terms rather than hyper-viscosity, for example, we do not develop a large inertial interval in our simulations, which are quite small. The modest inertial intervals in our simulations do not pose problems. We are interested in studying energy injection into a turbulent flow. Unlike properties which follow from scaling arguments, this is not an asymptotic property and does not require  $R \rightarrow \infty$ . Nevertheless we use several different simulations at different values of  $R$  to probe the robustness of our results. The simulations are done in a doubly-periodic box of the size,  $L = 2\pi$ , using a standard pseudo-spectral solver with full dealiasing. For the inverse cascade simulations, we used computational domains of sizes  $256^2$ ,  $512^2$  and  $1024^2$  in order to investigate the effects of varying Reynolds number. For comparison purposes, we also performed a small simulation of the direct cascade regime at a resolution of  $256^2$ . Time integration was done using a 3rd order Runge–Kutta integrator with integrating factors.

Unlike many numerical simulations of turbulence, the forcing term which we used is deterministic. It was designed to model the electromagnetic forcing which is a popular experimental method of driving turbulence in thin fluid layers [22, 24]. The idea is to place an array of magnets underneath the fluid layer in some particular arrangement. One then passes an electric current, which may have some non-trivial time dependence, through the fluid layer so that the Lorentz force produces a quasi-2D body force on the layer. Suppose that the electric current is applied in the x-direction. Denote it by  $\mathbf{I}(t) = I(t) \hat{\mathbf{x}}$ , with  $\hat{\mathbf{x}}$  being the unit vector in the x-direction. If  $\mathbf{B}(\mathbf{x}) = B(\mathbf{x}) \hat{\mathbf{z}}$  denotes the (vertical component of) the magnetic field generated by the magnet array, then the body force exerted on the fluid is

$$\mathbf{f}(\mathbf{x}, t) = g \mathbf{I}(t) \times \mathbf{B}(\mathbf{x}) \quad (2)$$

where  $g$  is a phenomenological coupling parameter which measures the strength of the coupling of the fluid to the magnetic field. Having applied the current in the x-direction, the force acts purely in the y-direction. In this article, we consider both the direct current (DC) case in which  $I(t)$  is independent of time and the alternating

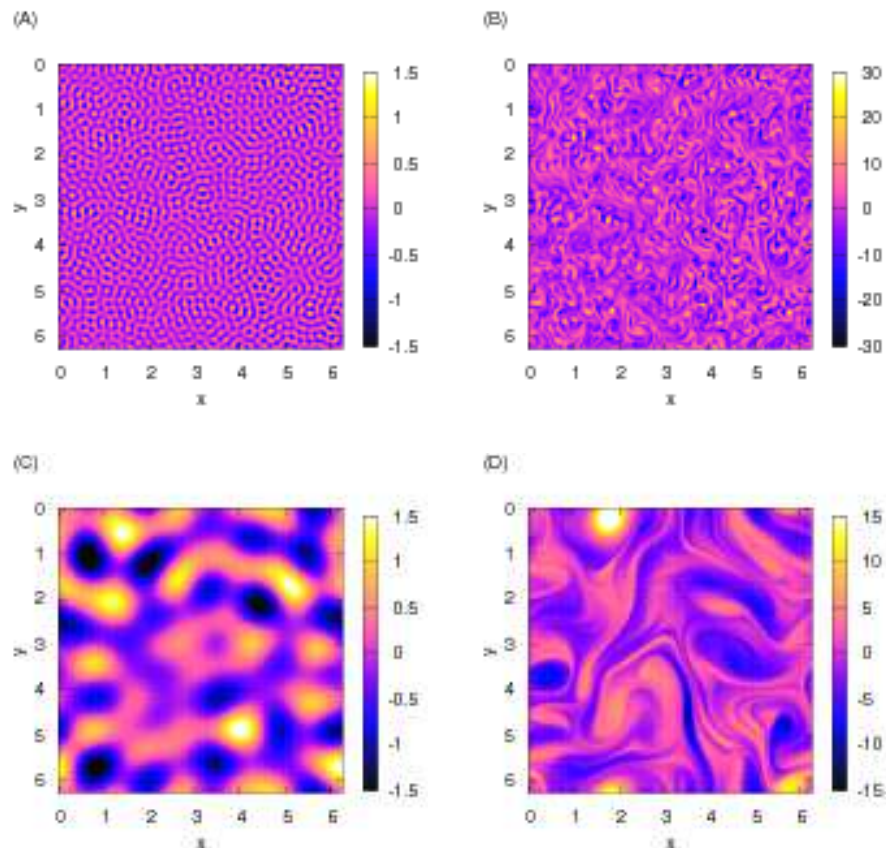


FIG. 1: (Color online)(A) Magnetic field used to force the (256x256) inverse cascade simulation. (B) Typical vorticity snapshot from the inverse cascade. (C) Magnetic field used to force the (256x256) direct cascade simulation. (D) Typical vorticity snapshot from the direct cascade.

current (AC) case where  $I(t)$  is a sinusoidal. Both are experimentally relevant. To produce an inverse cascade, the magnetic field is chosen to excite modes at small scales. For the direct cascade the magnetic field is chosen to excite modes at large scales Fig. 1(A) shows the magnetic field distribution,  $B(\mathbf{x})$ , used for forcing the inverse cascade simulations and Fig. 1(C) shows the corresponding field for the direct cascade simulations. The field  $B(\mathbf{x})$  is generated by choosing a sum of modes in spectral space clustered around some characteristic wavenumber. These modes are then assigned random phases and an inverse Fourier transform taken to produce a spatially disordered forcing field. The characteristic forcing wavenumbers are around 32, 64 and 128 for the inverse cascade simulations and around 3 for the direct cascade simulation. Note that, unlike some turbulence forcing schemes which employ a time-varying random forcing field, the disorder in our system is quenched. That is to say, once the initial random phases are assigned to produce a disordered magnetic field such as those shown in Figs. 1(A) and 1(C), the magnetic field remains fixed for the duration of the simulation.

Figs. 1(B) and 1(D) show instantaneous snapshots of the vorticity field for the inverse and direct cascades respectively at  $256^2$  resolution. Both are in the developed turbulence regime. The two fields are qualitatively very different. The inverse cascade vorticity field contains many small incoherent vortices at the scale of the forcing coexisting with larger scale clusters of like-sign vortices. The direct cascade vorticity field is dominated by a smaller number of more coherent vortices, which are again comparable in size to the forcing scale, separated by long ribbons.

The two regimes also differ qualitatively in spectral terms. Instantaneous energy spectra are shown in Fig. 2 and Fig.3. The inverse cascade spectrum is very close to the KLB prediction of  $k^{-5/3}$ , despite the fact that the simulation does not attempt to resolve the direct cascade range. It is accepted that the inverse cascade scaling of  $k^{-5/3}$  does not require an extensive direct cascade range despite the fact that it is required in the theoretical argument [20]. On the other hand, the direct cascade spectrum is much closer to  $k^{-4.5}$  than  $k^{-3}$ . This is again in agreement with extensive numerical and experimental

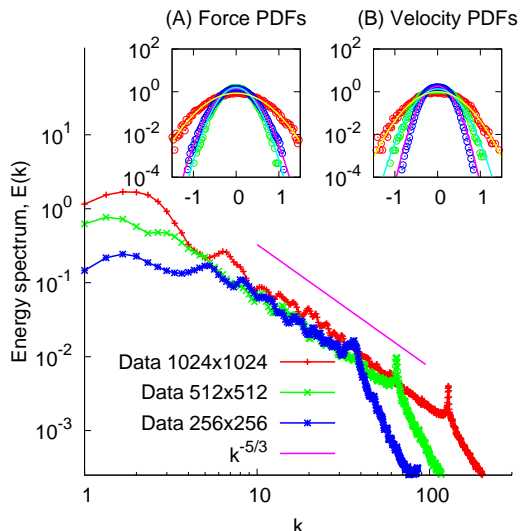


FIG. 2: (Color online) Snapshots of the energy spectra in the inverse cascade regime at resolutions of  $256^2$  (blue \*),  $512^2$  (red x) and  $1024^2$  (green o). Inset (A) shows the corresponding pdfs of the Lagrangian force and associated best fit Gaussian distributions. Inset (B) shows the corresponding pdfs of the Lagrangian velocity and associated best fit Gaussian distributions.

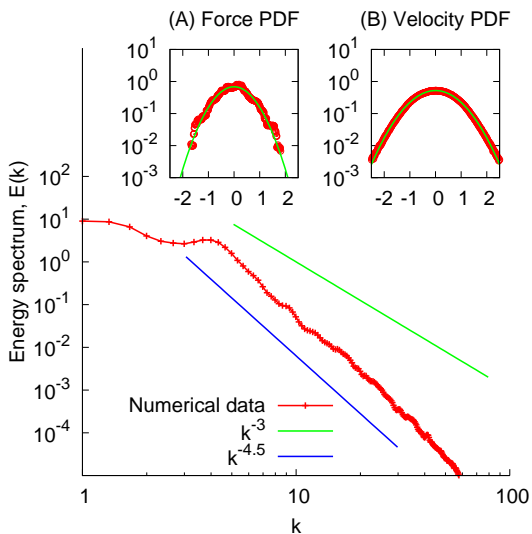


FIG. 3: (Color online) Snapshot of the energy spectrum in the inverse cascade regime at a resolution of  $256^2$ . Inset (A) shows the pdf of the Lagrangian force and associated best fit Gaussian distribution. Inset (B) shows the pdf of the Lagrangian velocity and associated best fit Gaussian distribution.

investigations of the direct cascade where it is typically found that the presence of the coherent vortices at large scales produces spectra which are steeper than the KLB prediction [25] and the  $k^{-3}$  is only observed when very large ranges are considered for both cascades [17].

When one talks about properties of parcels of fluid

moving in turbulence, it is natural to adopt a Lagrangian perspective. That is, one considers a set of  $N$  tracer particles, having positions,  $\mathbf{x}_i$ ,  $i = 1 \dots N$ , which follow the fluid flow passively. The tracer positions satisfy the advection equation:

$$\frac{d\mathbf{x}_i(t)}{dt} = \mathbf{v}(\mathbf{x}_i(t), t) \quad i = 1 \dots N \quad (3)$$

where  $\mathbf{v}(\mathbf{x}, t)$  is the solution of Eq. (1). To study the injection of energy into the turbulence from the forcing field, we computed the evolution of 100 such Lagrangian tracers. The Lagrangian power is defined

$$P(t) = \mathbf{v}(\mathbf{x}_i(t), t) \cdot \mathbf{f}(\mathbf{x}_i(t), t). \quad (4)$$

For our choice of forcing,  $\mathbf{f}$  is purely in the  $y$ -direction so that the power is a simple product rather than a dot product,  $P(t) = v_y(\mathbf{x}_i(t), t)f_y(\mathbf{x}_i(t), t)$ . We collected time series of  $v_y(\mathbf{x}_i(t), t)$  and  $f_y(\mathbf{x}_i(t), t)$  for each tracer. Multiplying these two together gave us a timeseries of the Lagrangian power. The velocity in a turbulent flow, be it Lagrangian or Eulerian, is a fluctuating quantity. Although the forcing field in Eq.(2) is deterministic, it is sampled along a random trajectory followed by the particles, so that  $f_y(\mathbf{x}_i(t), t)$  is also a fluctuating quantities. We computed the empirical probability distribution functions of both  $v_y(\mathbf{x}_i(t), t)$  and  $f_y(\mathbf{x}_i(t), t)$  from our numerical data. The resulting distributions are shown for the inverse cascade simulations in the insets of Fig. 2 and for the direct cascade simulations in the insets of Fig. 3. Both are close to Gaussian [26]. These results suggest that the Lagrangian power can be modeled as the product of two almost Gaussian variables which are presumably correlated to some degree [31]. We shall present measurements of the power in due course and test this assertion. First, however, we need some understanding of the probability distribution of products of correlated Gaussian variables. This is addressed in the next section.

### PRODUCTS OF NORMAL VARIABLES: CRAIG'S XY DISTRIBUTION

The product of two normally distributed random variables was first considered by Craig [27]. Consider two random variables,  $x$  and  $y$ , which follow a normal bivariate distribution with means  $\mu_x$  and  $\mu_y$  respectively, standard deviations  $\sigma_x$  and  $\sigma_y$  respectively and correlation coefficient  $\rho$ . Let  $Z = xy$ . In [27], an expression for the moment generating function of  $Z$  was derived and studied and the distribution function,  $\Pi_{xy}(Z)$ , was expressed as a difference of two integrals. For the purposes of the present work, we shall restrict ourselves to the case of zero means,  $\mu_x = \mu_y = 0$ , and derive  $\Pi_{xy}(Z)$  directly in a form appropriate for asymptotic analysis.

For this case the joint distribution of  $x$  and  $y$  is [28]

$$\Pi(x, y) = \frac{1}{2\pi\sigma_x\sigma_y\sqrt{1-\rho^2}} e^{-\frac{1}{2(1-\rho^2)}\left(\frac{x^2}{\sigma_x^2} - \frac{2\rho xy}{\sigma_x\sigma_y} + \frac{y^2}{\sigma_y^2}\right)}. \quad (5)$$

To obtain the distribution of  $Z$  we begin with the standard construction:

$$\Pi_{xy}(Z) = \mathbb{E}[\delta(xy - Z)] \quad (6)$$

$$= \frac{1}{2\pi} \int_{-\infty}^{\infty} dw e^{iZw} \mathbb{E}[e^{-ixyw}]. \quad (7)$$

Here, the expectation is with respect to the distribution (5). Calculating  $\mathbb{E}[e^{-ixyw}]$  is relatively simple:

$$\begin{aligned} \mathbb{E}[e^{-ixyw}] &= \int_{-\infty}^{\infty} dx \int_{-\infty}^{\infty} dy \Pi(x, y) e^{-ixyw} \\ &= \frac{1}{2\pi\sigma_x\sigma_y\sqrt{1-\rho^2}} \int d\mathbf{x} e^{-\frac{1}{2}\mathbf{x}\cdot A(w)\mathbf{x}}, \end{aligned} \quad (8)$$

where  $\mathbf{x} = (x, y)$  and

$$A(w) = \begin{pmatrix} \frac{1}{\sigma_x^2(1-\rho^2)} & iw - \frac{\rho}{\sigma_x\sigma_y(1-\rho^2)} \\ iw - \frac{\rho}{\sigma_x\sigma_y(1-\rho^2)} & \frac{1}{\sigma_y^2(1-\rho^2)} \end{pmatrix}. \quad (9)$$

Evaluating the integral in Eq.(8) is a straightforward application of Gaussian integration (see, for example [29]):

$$\int d\mathbf{x} e^{-\frac{1}{2}\mathbf{x}\cdot A(w)\mathbf{x}} = \sqrt{\frac{(2\pi)^2}{\det A(w)}} \quad (10)$$

$$= \frac{2\pi}{\sqrt{(w+i\Lambda^-)(w+i\Lambda^+)}} \quad (11)$$

where

$$\Lambda^+ = \frac{1}{\sigma_x\sigma_y(1+\rho)} \quad (12)$$

$$\Lambda^- = \frac{1}{\sigma_x\sigma_y(1-\rho)}. \quad (13)$$

We are left with the following expression for the product distribution:

$$\Pi_{xy}(Z) = \frac{\sqrt{\Lambda^+\Lambda^-}}{2\pi} \int_{-\infty}^{\infty} \frac{e^{iZw} dw}{\sqrt{(w-i\Lambda^+)(w+i\Lambda^-)}}. \quad (14)$$

This integral cannot generally be expressed in terms of elementary functions, except in the case of  $\rho = 0$ . In this case,  $\Lambda^- = \Lambda^+ = 1/(\sigma_x\sigma_y)$  and Eq.(14) becomes proportional to one of the integral representations of the zeroth order modified Bessel function of the second kind [30] :

$$\Pi_{xy}(Z) = \frac{2}{\pi\sigma_x\sigma_y} K_0\left(\frac{Z}{\sigma_x\sigma_y}\right). \quad (15)$$

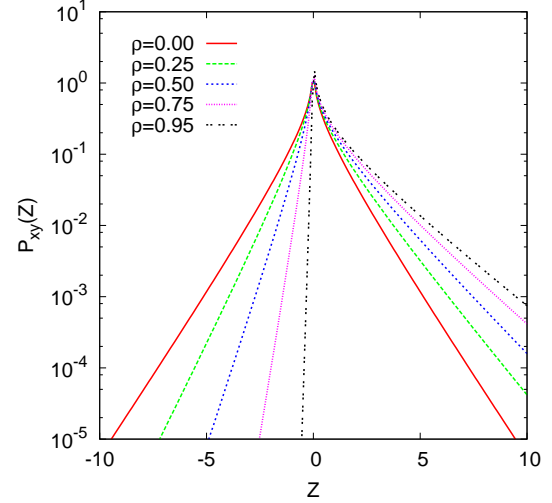


FIG. 4: (Color online) Craig's XY-distribution for different values of  $\rho$ .

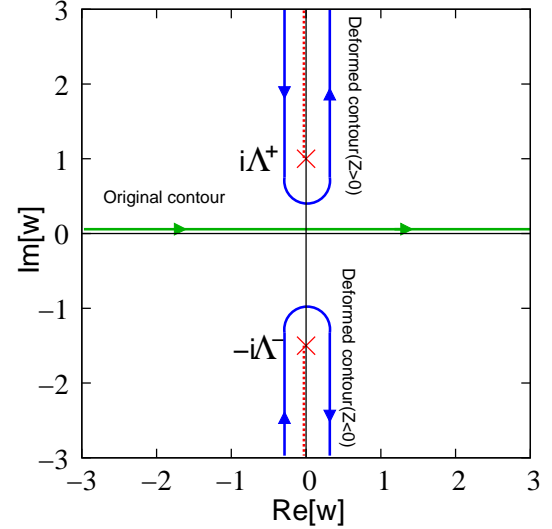


FIG. 5: (Color online) Integration contours for Eq.(14).

For general values of  $\rho$ , the integral can be evaluated numerically. Some curves are shown for a range of positive values of  $\rho$  in Fig.4. We remark that the pdf is always peaked at zero with asymmetric exponential tails. The degree of asymmetry increases with increasing  $\rho$ . This asymmetry reflects the fact that as the degree of correlation between  $x$  and  $y$  increases, they are increasingly likely to have the same sign. This ensures that the probability of a positive value for the product increases with increasing  $\rho$  while the probability of a negative value decreases. For negative values of  $\rho$ , or anti-correlation between  $x$  and  $y$ , the asymmetry is in the opposite sense.

Although we cannot evaluate  $\Pi_{xy}(z)$  in general, it is

possible to calculate the asymptotic behaviour for large absolute values of  $Z$  for any  $\rho$ . Let us look at the structure of the integrand in Eq.(14) in the complex  $w$ -plane. The analytic landscape is shown in Fig. 5. There are two singularities on the imaginary axis at  $i\Lambda^+$  and  $-i\Lambda^-$ . The square root necessitates the introduction of a branch cut joining these two singularities which we take to be along the imaginary axis at  $(i\Lambda^+, i\infty]$  and  $[-i\infty, -i\Lambda^-)$ . Depending on the sign of  $Z$ , we deform the original contour of integration along the real axis into either the upper or lower complex plane as shown in Fig. 5. Careful study of the integrand reveals that it acquires a phase difference of  $\pi$  upon going from one side of the branch cut to the other. Considering the case  $Z > 0$ , we may thus write:

$$\Pi_{xy}(Z) = \frac{\sqrt{\Lambda^+\Lambda^-}}{2\pi} \left[ \int_{i\Lambda^+}^{i\infty} \frac{e^{iZw} dw}{\sqrt{(w+i\Lambda^+)(w-i\Lambda^-)}} + e^{i\pi} \int_{i\infty}^{i\Lambda^+} \frac{e^{iZw} dw}{\sqrt{(w+i\Lambda^+)(w-i\Lambda^-)}} \right].$$

Rescaling  $w \rightarrow iw$  and putting the two integrals together we get

$$\Pi_{xy}(Z) = \frac{\sqrt{\Lambda^+\Lambda^-}}{\pi} \int_{\Lambda^+}^{\infty} \frac{e^{-Zw} dw}{\sqrt{(w-\Lambda^+)(w+\Lambda^-)}}. \quad (16)$$

Changing variables,  $w = \Lambda^+ + \frac{u}{Z}$  and performing some algebra, we can write this in the form

$$\Pi_{xy}(Z) = \frac{1}{\pi} \sqrt{\frac{\Lambda^+\Lambda^-}{\Lambda^+\Lambda^-}} \frac{e^{-\Lambda^+Z}}{\sqrt{Z}} \int_0^{\infty} du u^{-\frac{1}{2}} e^{-u} \times \left[ 1 + \frac{u}{(\Lambda^+\Lambda^-)Z} \right]^{-\frac{1}{2}}. \quad (17)$$

To finally obtain an asymptotic series, we expand the last factor using the Binomial Theorem and integrate term by term (recalling the definition of the Gamma function:  $\Gamma(x) = \int t^{x-1} e^{-t} dt$ ). We obtain:

$$\Pi_{xy}(Z) = \frac{1}{\pi} \sqrt{\frac{\Lambda^+\Lambda^-}{\Lambda^+\Lambda^-}} \frac{e^{-\Lambda^+Z}}{\sqrt{Z}} \times \sum_{k=0}^{\infty} \binom{-\frac{1}{2}}{k} \Gamma(k + \frac{1}{2}) (\Lambda^+\Lambda^-)^{-k} Z^{-k}. \quad (18)$$

Following the same approach for  $Z < 0$ , taking the deformed contour in the lower half plane, we obtain a very similar formula with  $\Lambda^+$  and  $\Lambda^-$  interchanged and  $Z$  replaced by  $|Z|$ . Noting that  $\Gamma(\frac{1}{2}) = \sqrt{\pi}$ , the leading order asymptotic behaviour for large absolute values of  $Z$  is found to be:

$$\Pi_{xy}(Z) \sim \begin{cases} \sqrt{\frac{\Lambda^+\Lambda^-}{\pi(\Lambda^+\Lambda^-)}} \frac{e^{-\Lambda^+Z}}{\sqrt{Z}} & Z > 0 \\ \sqrt{\frac{\Lambda^+\Lambda^-}{\pi(\Lambda^+\Lambda^-)}} \frac{e^{-\Lambda^-|Z|}}{\sqrt{|Z|}} & Z < 0 \end{cases} \quad (19)$$

The strong cusp at zero is the second striking feature of the pdfs shown in Fig. 4. Let us briefly investigate the behaviour of the integral in Eq.(14) near  $Z = 0$ . A fast way to compute the leading behaviour as  $Z \rightarrow 0$  is to make the change of variables  $w = \Lambda^+ + u$  in Eq.(16), then differentiate the resulting expression with respect to  $Z$  and apply the integrating factor  $e^{\Lambda^+Z}$ , to obtain the following differential equation:

$$\frac{d}{dZ} \left( e^{\Lambda^+Z} \Pi_{xy}(Z) \right) = -\frac{\sqrt{\Lambda^+\Lambda^-}}{\pi} \int_0^{\infty} \frac{ue^{-Zu} du}{\sqrt{u(u+\Lambda^+\Lambda^-)}} \quad (20)$$

Putting the integral on the right into Mathematica, we find that it can be expressed in terms of a confluent hypergeometric function of the second kind which has a tabulated Taylor expansion for small values of its argument [28] :

$$\int_0^{\infty} \frac{ue^{-Zu} du}{\sqrt{u(u+\Lambda^+\Lambda^-)}} = \frac{\sqrt{\pi}}{2Z} U\left(\frac{1}{2}, 0, (\Lambda^+\Lambda^-)Z\right) = \frac{\sqrt{\pi}}{2(\Lambda^+\Lambda^-)Z} \frac{2}{\sqrt{\pi}} + O(1).$$

Sustituting this back into Eq.(20) and integrating term by term gives, to leading order in  $Z$ :

$$\Pi_{xy}(Z) \sim -\frac{\sqrt{\Lambda^+\Lambda^-}}{\pi} \log Z + O(1). \quad (21)$$

Note that this simplistic approach does not provide an obvious way of determining the constant which arises upon integrating Eq.(20). Thus we do not obtain the subleading terms in the expansion near zero. For this, a more sophisticated analysis will be required. Nevertheless, this quick calculation is sufficient to demonstrate that the product distribution is logarithmically singular near zero. Further, we note that, to leading order, the singularity is symmetric about zero.

## STATISTICS OF LAGRANGIAN POWER (DIRECT CURRENT)

Let us now return to the Lagrangian power. We have seen from the insets of Fig. 2 and Fig. 3 that in both the inverse and direct cascade regimes, both the velocity and force are close to Gaussian in the Lagrangian frame. Some sample time series of the product of the two, the Lagrangian power, are shown in Fig. 6. We see that both traces exhibit wild fluctuations, both positive and negative. The timeseries look far from Gaussian, as one might expect from the discussion of the previous section.

It is clear from Eq.(14) that  $\sigma_x \sigma_y \Pi_{xy}(\sigma_x \sigma_y Z)$  is a function of  $\rho$  only. Therefore, in plotting the numerical data, we use this rescaling together with the values of the standard deviations presented in Table I, to collapse all of our

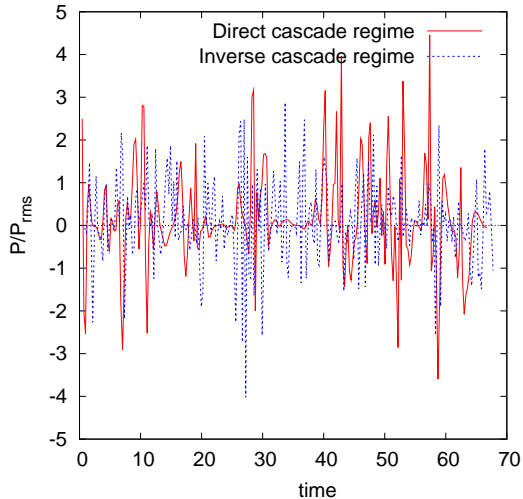


FIG. 6: (Color online) Typical timetraces of the Lagrangian power in the direct (red solid line) and inverse (blue dashed line) cascade regimes normalized by their rms values.

data to similar curves. The rescaled empirical distribution functions of the power for both direct and inverse cascades at  $256^2$  resolution are shown in Fig. 7. They almost collapse to the same curve and are qualitatively similar to Craig's XY-distribution shown in Fig. 4. They are strongly peaked at zero with asymmetric exponential tails. The positive tail decays more slowly than the negative tail which gives the distribution and net positive mean value, despite the fact that the most probable value is zero. The peak at zero is consistent with the logarithmic singularity suggested by Eq.(21) but such a divergence is too weak to observe unambiguously with resolution we were able to achieve for the pdf near zero.

Simulation	$v_{rms}$	$\nu$	$R$	$\sigma_f^2$	$\sigma_v^2$	$\rho$
IC $256^2$	0.32	$2.9 \times 10^{-4}$	$6.8 \times 10^3$	0.082	0.047	0.11
IC $512^2$	0.42	$7.3 \times 10^{-5}$	$3.6 \times 10^4$	0.063	0.086	0.056
IC $1024^2$	0.57	$1.8 \times 10^{-5}$	$2.0 \times 10^5$	0.21	0.16	0.027
DC $256^2$	1.0	$5.8 \times 10^{-4}$	$1.1 \times 10^4$	0.34	0.59	0.14

TABLE I: Parameters of the inverse cascade (IC) and direct cascade (DC) simulations to two significant digits. The columns are, from left to right, r.m.s. velocity,  $v_{rms}$ , kinematic viscosity,  $\nu$ , Reynolds number,  $R = 2\pi v_{rms}/\nu$ , variance of the Lagrangian force,  $\sigma_f^2$ , variance of the Lagrangian velocity,  $\sigma_v^2$ , force-velocity correlation coefficient,  $\rho$ .

To make this more quantitative, we should compare the empirical distributions with Eq.(14) and Eq.(18), taking  $x$  to be the force and  $y$  to be the velocity. Table I shows the measured values of the correlation coefficient,  $\rho$ , between the force and velocity and their standard deviations,  $\sigma_f$  and  $\sigma_v$ . Fig. 7 also includes plots of the tails predicted from Eq.(19), for the measured  $\rho$  values shown

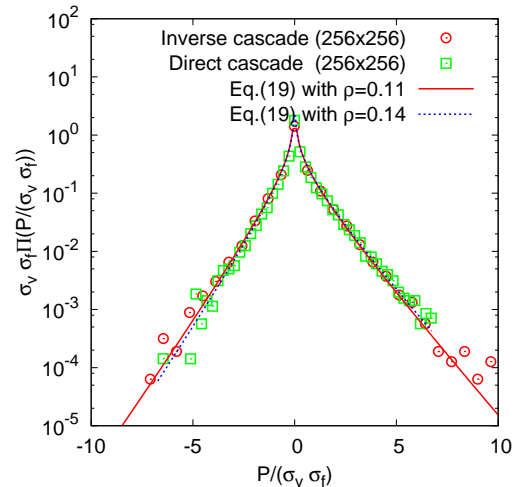


FIG. 7: (Color online) Rescaled empirical pdfs of Lagrangian power for both the inverse (red +) and direct (green x) cascades at  $256^2$  resolution. Solid lines indicate the tails predicted by Eq.(19) for the measured values of the  $v$ - $f$  correlation coefficient,  $\rho$ .

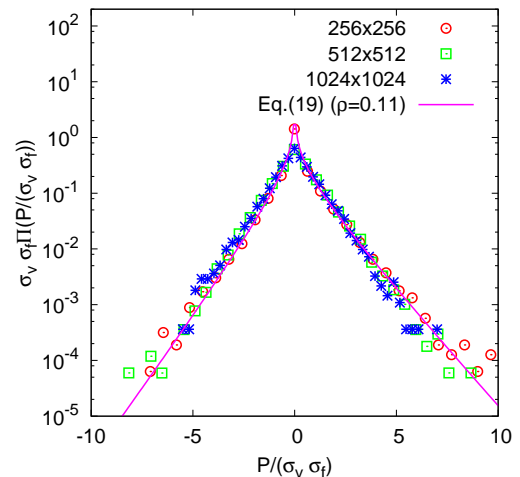


FIG. 8: (Color online) Rescaled empirical pdfs of Lagrangian power for the inverse cascade at resolutions of  $256^2$  (red o),  $512^2$  (green x) and  $1024^2$  (blue \*) with corresponding Reynolds numbers as noted in Table I. The solid line indicates the tails predicted by Eq.(19) for the most asymmetric case ( $256^2$ ) having  $\rho = 0.11$ .

in Table I. In fact, the curves obtained for  $\rho = 0.11$  and  $\rho = 0.14$  are almost impossible to distinguish at the level of convergence which we have been able to obtain from our data. Notwithstanding the question of why the values of  $\rho$  should be so close for the two regimes, both show excellent agreement for the tails of the power distribution, confirming our qualitative arguments that the

pdf should be close to Craig's XY-distribution.

Next we investigate whether Craig's XY-distribution remains a good model of the power pdf as the Reynolds number is increased. Fig. 8 shows the rescaled pdfs of the power obtained for the three inverse cascade simulations at resolutions of  $256^2$ ,  $512^2$  and  $1024^2$ . The corresponding Reynolds numbers are shown in Table I. It is clear from Fig. 8 that the three pdfs almost rescale to the same curve. There is a discernible trend towards decreasing asymmetry as the Reynolds number is increased which is reflected in the decreasing value of the correlation coefficient,  $\rho$ . This is to be expected intuitively. As the velocity becomes more turbulent, it becomes less correlated with the forcing field. Given that we have established that the average power injected is non-zero due to the asymmetry of the tails, one might wonder whether the average power also decreases as  $R$  increases and the tails grow more symmetric. In fact the mean of the XY-distribution is  $\sigma_v \sigma_f \rho$  so a decreasing  $\rho$  can be compensated for by increasing the variance of the velocity as  $R$  increases to maintain a constant rate of energy injection. Nevertheless, it would be interesting to understand exactly how  $\rho$  decreases with increasing  $R$ . The simulations presented here, while sufficient to identify the trend, are clearly insufficient to answer this question quantitatively.

One final point should be made about Fig. 8 which clearly illustrates the limitations of this kind of modeling. While the data from the  $256^2$  simulations shown in Fig. 7 are almost perfectly fitted by Eq.(18), the  $512^2$  and  $1024^2$  simulations show a smoothing out of the logarithmic cusp at zero, although the tails remain quite well captured. The XY-distribution only describes the power pdf as well as the underlying force and velocity distributions can be approximated by Gaussian distributions. Close inspection of the velocity pdfs for the higher resolution inverse cascade simulations indicate that the pdfs of velocity become slightly flatter than Gaussian near zero. This variation presumably accounts for the smoothing of the cusp. One might speculate about the physical meaning of this deviation but that is not the purpose of the present work. Indeed, in the following section, we shall see that large deviations from Gaussianity for the forcing field can result from simple modifications of the experimental set up.

### STATISTICS OF LAGRANGIAN POWER (ALTERNATING CURRENT)

Although a Gaussian forcing field of the type observed in the direct current simulations is often observed experimentally, and is often imposed theoretically in order to simplify calculations, it is by no means true that the forcing must be Gaussian. Thus, while the results derived above may be applicable to a range of situations, we do not claim that they are in any way universal. One

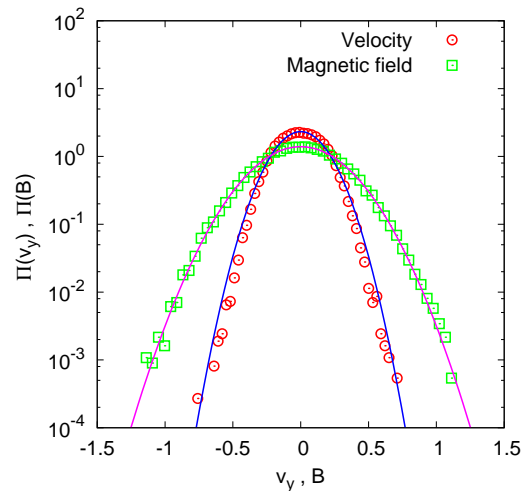


FIG. 9: (Color online) Pdfs of the magnetic field (green +) and velocity (red o) in the Lagrangian frame for the inverse cascade regime with AC driving.

of the simplest ways to produce a non-Gaussian forcing is to apply AC current. We shall study this case in this section in somewhat less detail than the DC case. The principle aim is to compare with the Gaussian case where we believe that the simple product distribution discussed above provides a good model of turbulent power fluctuations. For the AC simulations discussed below we take the current to be  $I(t) = \cos(2\pi\omega t)$  with  $\omega = 10$ .

For the case of AC driving, the Lagrangian force is itself a product of a non-trivial current and a magnetic field:

$$f_y(t) = I(t)B(t). \quad (22)$$

Let us assume that  $B(t)$  remains Gaussian. This assumption is well supported by the numerical measurements. Fig. 9 shows the magnetic field and velocity distributions for the inverse cascade regime driven by an alternating current. Both remain close to Gaussian as in the direct current case. So, given that  $B(t)$  is Gaussian, how is the product  $f(t) = I(t)B(t)$  distributed? Of course, to definitively answer this question we would need to understand if and how the magnetic field is correlated with the current. However the simplest approximation is to assume they are uncorrelated, another assumption which is supported by our measurements. In this case, we may treat  $I(t)$  as a random variable generated by uniformly sampling the phase,  $\omega t$  over the interval  $[0, \frac{2\pi}{\omega}]$ . If we proceed with the calculation, this leads after some simple manipulations to the following expression for the pdf of  $I$ :

$$\Pi_I(I) = \int_{-\infty}^{\infty} \frac{dw}{2\pi} e^{i w I} J_0(w), \quad (23)$$



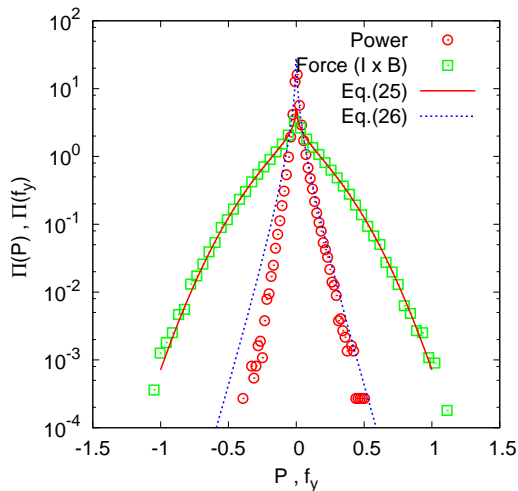


FIG. 10: (Color online) Pdfs of the Lagrangian force (green  $\square$ ) and power (red  $\circ$ ) for the inverse cascade regime with AC driving.

where  $J_0(w)$  is the zeroth order Bessel function of the first kind. This integral has a name - Weber's Discontinuous Integral (see [30], chap. IV), and can be evaluated as follows:

$$\Pi_I(I) = \begin{cases} \frac{1}{\sqrt{1-I^2}} & \text{if } |I| < 1 \\ 0 & \text{if } |I| \geq 1 \end{cases} \quad (24)$$

This distribution makes sense. The current is a cosine and cannot take values outside of the range  $[-1, 1]$ . Furthermore, the most probable values are  $\pm 1$  since this is where the cosine function is flattest. Let us now combine this distribution with an assumed Gaussian distribution for  $B(t)$  with mean zero and variance  $\sigma_B$ . Doing some lengthy, but elementary, calculations in the spirit of our derivation of  $\Pi_{xy}(Z)$ , we obtain the following proposed distribution for the Lagrangian force in the case of AC driving:

$$\Pi_f^{(\text{ac})}(F) = \frac{1}{2\pi} \sqrt{\frac{2}{\pi\sigma_B^2}} e^{-\frac{F^2}{4\sigma_B^2}} K_0\left(\frac{F^2}{4\sigma_B^2}\right). \quad (25)$$

This formula is compared with the measured Lagrangian force distribution in Fig 10. We see that the alternating current strongly modifies the distribution of the force from the Gaussian distribution measured in the direct current case. However, this modification is correctly captured by Eq.(25).

Finally, one may ask if the distribution of the power may be calculated in this case. Here one encounters a problem. We have learned that the correlation coefficient between the force and the velocity controls the degree of asymmetry of the power pdf. In the direct current case, where both the force and the velocity are Gaussian,

the bivariate normal distribution, Eq.(5), provides a very reasonable way to correlate the two. In the alternating current case, where the force follows the distribution of Eq.(25), it is less obvious how to correlate the two. In the absence of a more thorough analysis addressing this issue, we give here the result for the uncorrelated case only. If the force follows the distribution Eq.(25) with standard deviation  $\sigma_B$  for the magnetic component and the velocity is normally distributed with standard deviation,  $\sigma_v$ , then some lengthy calculations show that the uncorrelated product follows the distribution

$$\Pi^{(\text{ac})}(P) = \frac{1}{\pi\sigma_B\sigma_v} \int_{-\infty}^{\infty} \frac{dw}{w} e^{-\left(\frac{F^2}{2\sigma_v^2 w^2} + \frac{w^2}{4\sigma_B^2}\right)} K_0\left(\frac{w^2}{4\sigma_B^2}\right) \quad (26)$$

This distribution is plotted with the measured values of  $\sigma_B$  and  $\sigma_v$  in Fig 10 against the empirical distribution of the Lagrangian power. As expected, it completely fails to capture the asymmetry of the power distribution. Nevertheless it is sufficiently close to convince us that the heuristic arguments presented here are correct and that some more careful calculations might be worth doing to attempt to incorporate the correlation between  $v$  and  $f$  in a reasonable way. Furthermore, the measured distribution for the power looks qualitatively very similar to the distributions measured for the direct current case. This is despite the fact that the force distributions are so different in the two cases. This suggests that some qualitative features of the distribution are more universal than one might expect from the very particular calculations performed above for products of Gaussian variables. These questions may be worth further investigation in the future.

## CONCLUSIONS

We have characterised the injection of energy into a two-dimensional flow by measuring the injected power in the Lagrangian frame. The measured distribution is very sharply peaked at zero with asymmetric exponential tails. It can be understood as arising from a simple product of correlated almost-Gaussian variables (the force and the velocity). From our analysis, we suggest that the power distribution is actually logarithmically singular at zero although this is too weak of a divergence to distinguish convincingly in our numerical data. We derived an asymptotic expression for the degree of asymmetry of the tails of the power distribution which depends only on the correlation coefficient of the force and velocity. We concluded by comparing the results for a case, alternating current instead of direct current forcing, for which the observed force distribution is far from Gaussian. The qualitative features of the power pdf remain unchanged although it will be hard to quantify the measurements as easily as in the Gaussian case.

### Acknowledgements

This work was carried out under the auspices of the National Nuclear Security Administration of the U.S. Department of Energy at Los Alamos National Laboratory under Contract No. DE-AC52-06NA25396. We would like to acknowledge many helpful discussions with our colleagues, particularly M. Chertkov, R. Ecke, M. Rivera, R. Teodorescu and O. Zaboronski.

---

\* Corresponding Author: mbandi@lanl.gov

† Electronic address: connaughtonc@gmail.com

- [1] H. Schlichting, *Boundary-layer theory* (New York; McGraw-Hill, 1979).
- [2] D. Lathrop, J. Fineberg, and H. Swinney, *Phys. Rev. A* **46**, 6390 (1992).
- [3] R. Labbé, J.-F. Pinton, and S. Fauve, *J. Phys. II France* **6**, 1099 (1996).
- [4] J. Titon and O. Cadot, *Phys. Fluids* **15**, 625 (2003).
- [5] T. Toth-Katona and J. T. Gleeson, *Phys. Rev. Lett.* **91**, 264501 (2003).
- [6] E. Falcon, S. Aumaître, C. Falcón, C. Laroche, and S. Fauve, *Phys. Rev. Lett.* **100** (2008).
- [7] S. Aumaître and S. Fauve, *Europhys. Lett.* **62**, 822 (2003).
- [8] D. Evans, E. Cohen, and G. Morris, *Phys. Rev. Lett.* **71**, 2401 (1993).
- [9] G. Gallavotti and E. Cohen, *Phys. Rev. Lett.* **74**, 2694 (1995).
- [10] J. Kurchan, *J. Phys. A* **31**, 3719 (1998).
- [11] V. Chernyak, M. Chertkov, and C. Jarzynski, *J. Stat. Phys.* **8**, 08001 (2006).
- [12] M. Bandi and C. Connaughton (2007), arXiv:0710.3368 [cond-mat.stat-mech].
- [13] R. H. Kraichnan, *Phys. Fluids* **10**, 1417 (1967).
- [14] C. E. Leith, *Phys. Fluids* **11**, 671 (1968).
- [15] G. K. Batchelor, *Phys. Fluids* **12**, 233 (1969).
- [16] U. Frisch, *Turbulence: The Legacy of A. N. Kolmogorov* (Cambridge University Press, Cambridge, 1995).
- [17] G. Boffetta, ArXiv e-prints (2006), nlin.CD/0612035.
- [18] C. H. Bruneau and H. Kellay, *Phys. Rev. E* **71**, 046305 (2005).
- [19] H. Kellay and W. I. Goldburg, *Rep. Prog. Phys.* **65**, 845 (2002).
- [20] C. Tran and J. Bowman, *Phys. Rev. E* **69**, 036303 (2004).
- [21] G. Boffetta, A. Celani, and M. Vergassola, *Phys. Rev. E* **61**, R29 (2000).
- [22] M. Rivera, W. Daniel, and R. Ecke (2005), eprint: arXiv:cond-mat/0512214, arXiv:cond-mat/0512214.
- [23] S. Chen, R. Ecke, G. Eyink, M. Rivera, X. Wang, and Z. Xiao, *Phys. Rev. Lett.* **96**, 084502 (2006).
- [24] J. Paret and P. Tabeling, *Phys. Fluids* **10**, 3126 (1998).
- [25] C. Beta, K. Schneider, and M. Farge, *Commun. Nonlin. Sci. Num. Simulation* **8**, 537 (2003).
- [26] O. Kamps and R. Friedrich (2007), arXiv:0710.1739v1 [physics.flu-dyn].
- [27] C. Craig, *Ann. Math. Statist.* **7**, 1 (1937).
- [28] M. Abramowitz and I. Stegun, *Handbook of mathematical functions, with formulas, graphs, and mathematical tables* (Dover: New York, 1965).
- [29] C. Itzykson and J.-M. Drouffe, *Statistical Field Theory Vol. 1* (Cambridge, UK: Cambridge University Press, 1991).
- [30] F. Bowman, *Introduction to Bessel Functions* (New York: Dover, 1958).
- [31] Describing the pdf of injected power using two correlated normal variables has also been proposed independently by E. Falcon, S. Aumaître, C. Falcón, C. Laroche and S. Fauve [6]